minerals

MDPI

Article

Carbonate U-Pb Geochronology and Clumped Isotope Constraints on the Origin of Hydrothermal Dolomites: A Case Study in the Middle Permian Qixia Formation, Sichuan Basin, South China

Yu Zou [1,2], Donghua You [1,2,*], Bo Chen [3,*], Huamin Yang [1,2], Zhixing Tian [3], Dongna Liu [4] and Liyu Zhang [1,2]

[1] State Key Laboratory of Shale Oil and Gas Enrichment Mechanisms and Effective Development, SINOPEC, Beijing 100083, China
[2] Key Laboratory of Petroleum Accumulation Mechanisms, SINOPEC, Wuxi 214126, China
[3] Nanjing Institute of Geology and Palaeontology, Chinese Academy of Sciences, Nanjing 210008, China
[4] College of Mining Engineering, Taiyuan University of Technology, Taiyuan 030024, China
* Correspondence: youdh.syky@sinopec.com (D.Y.); chenbo@nigpas.ac.cn (B.C.)

Abstract: Reservoirs in the dolomites of the Middle Permian Qixia Formation in the Sichuan Basin are currently important oil and gas exploration objects in China. However, the questions concerning the sources of the dolomitized fluids and the control factors of the Qixia hydrothermal dolomites remain unclear. In this study, the original hydrothermal dolomites (the replacement dolomites (RDs) and saddle dolomites (SDs)) from the Qixia Formation in the southwestern Sichuan Basin (the PR1 well and Baoxing section) were mainly examined using novel in situ carbonate U-Pb dating with clumped isotopes (Δ_{47}). Our results show that the U-Pb ages of the latest SDs from the PR1 well (located in the middle zone of the Emeishan large igneous province (ELIP) and distanced from the Orogenic Belt of Longmenshan) are 257.9–251.0 Ma, coincident with the period of main activity of the ELIP. Combined with the previous U-Pb dating, we propose that the high-temperature $T_{\Delta47}$ (82.2–108.4 °C and 127.5–205.9 °C) recorded for SDs from the PR1 well and Baoxing section may have responded to ELIP activity and Longmenshan orogeny activity, respectively. In addition, in the entire southwestern Sichuan Basin, the RDs and SDs yield similar $\delta^{13}C$ and $\delta^{18}O$ values, indicating that the dolomites were formed by hydrothermal fluids of similar sources, with marine hydrothermal fluids being a highly possible source. Finally, this study proposes a new hydrothermal dolomite genesis model for the Qixia Formation, emphasizing that the formation of hydrothermal dolomites mainly depends on the proximity to tectonic thermal events in space and time.

Keywords: hydrothermal dolomitization; Qixia Formation; U-Pb dating; clumped isotopes

check for updates

Citation: Zou, Y.; You, D.; Chen, B.; Yang, H.; Tian, Z.; Liu, D.; Zhang, L. Carbonate U-Pb Geochronology and Clumped Isotope Constraints on the Origin of Hydrothermal Dolomites: A Case Study in the Middle Permian Qixia Formation, Sichuan Basin, South China. *Minerals* **2023**, *13*, 223. https://doi.org/10.3390/min13020223

Academic Editors: Luis Miguel Nieto and José Miguel Molina

Received: 12 January 2023
Revised: 31 January 2023
Accepted: 1 February 2023
Published: 3 February 2023

Copyright: © 2023 by the authors. Licensee MDPI, Basel, Switzerland. This article is an open access article distributed under the terms and conditions of the Creative Commons Attribution (CC BY) license (https://creativecommons.org/licenses/by/4.0/).

1. Introduction

Dolomite reservoirs in the Middle Permian Qixia Formation represent one of the most important oil and gas exploration targets in the Sichuan Basin, South China—especially in its western part, where high-yield natural gas flows have been obtained from many wells, showing great exploration potential [1,2]. Many studies have been carried out using multiple methods—including rock mineralogy, as well as elemental and isotopic geochemical analyses—to reconstruct the mechanisms of formation of the Qixia dolomites. Consequently, various models have been proposed, including mixed-water dolomitization [3], burial-metasomatic dolomitization, and hydrothermal dolomitization [4,5]. In the Qixia Formation, the porphyritic and saddle-shaped dolomites that fill fissures and vugs are the most common type of dolomite. These rocks are considered to be hydrothermal in origin and are widely distributed across the Sichuan Basin. Their development and distribution characteristics could have played a key role in dissolving surrounding rocks and forming sealing traps, which act as important hydrothermal dolomite reservoirs [6].

Most authors agree that the dolomites in the Qixia Formation are hydrothermal in origin; however, considerable controversies exist regarding the properties of the hydrothermal fluids, the formation temperature, and the responsible thermal events. Some scholars suggest that the hydrothermal fluids are mainly derived from seawater [7], whereas others believe that they are influenced by deep magmatic hydrothermal fluids [8]. Li et al. [9] further proposed that the fluid properties may have significantly varied in space, observing obvious spatial differences in the original rock texture and fault systems, as well as in the degree of hydrothermal dolomitization within the Sichuan Basin. These previous studies usually measured a uniform temperature for fluid inclusions to estimate the formation temperature of the hydrothermal dolomites [6], but due to the influence of late diagenesis, this method suffers from limitations hindering the reconstruction of accurate dolomite formation temperatures as well as dolomitization fluid characteristics (e.g., $\delta^{18}O$ values). There are two main opinions as to which thermal events were responsible for the formation of the hydrothermal dolomite in the Qixia Formation: some authors consider the strong volcanism of the Emeishan large igneous province (ELIP) in the late Middle Permian as the main cause [5,8], whereas others believe that the dolomitization was initiated by tectonic events within the Longmenshan Orogenic Belt starting in the Late Triassic [10,11]. The differentiation between these two tectonic thermal events is not only important for the identification of the formation time and geodynamic background of the hydrothermal dolomites, but also affects the accurate reconstruction of the formation and evolution process of the hydrothermal dolomite reservoir.

In order to resolve these open questions described above, it is necessary to know the precise time of formation and the properties of the diagenetic fluids for the Qixia hydrothermal dolomites. Laser ablation inductively coupled plasma mass spectrometry (LA-ICP-MS) is commonly used for in situ U-Pb dating of carbonate minerals such as primary sediments [12], reservoir pore/fracture packing, or cement [13,14]. Compared to the acid digestion–isotope dilution (ID) method [15], in situ analysis has higher spatial resolution and, thus, can accurately determine the formation age of diagenetic carbonate minerals [16]. Furthermore, the abundance of $^{13}C^{18}O^{16}O$-bonds in carbonate minerals is correlated with the mineral growth temperature, but it is not connected to the oxygen and carbon isotopic composition or fluid $\delta^{18}O$ values in which the minerals grew [17]. Thus, the carbonate clumped isotope (denoted as Δ_{47}) analysis is an independent method for paleotemperature reconstruction [18,19]. The combination of the growth temperature for the analyzed mineral based on clumped isotope analysis ($T_{\Delta 47}$) and the $\delta^{18}O$ value of the mineral enables us to calculate the $\delta^{18}O$ composition of the fluid during carbonate growth, providing an independent constraint on the fluid properties [18]. In this study, we carried out a combined in situ U-Pb carbonate dating and clumped isotope analysis of the hydrothermal dolomites of the Qixia Formation from both field outcrops and a drilling core in the southwestern Sichuan Basin. Our main purpose was to establish the cause–effect relationship between the formation of hydrothermal dolomites and the evolution of regional tectonic thermal events, thereby providing a theoretical basis for the analysis of regional oil and gas accumulation.

2. Geological Setting

The Sichuan Basin is situated in the northwestern part of the Yangtze Platform in South China. After experiencing a sedimentary discontinuity caused by uplift and denudation in the Early Permian, a major transgression began in the Middle Permian. Subsequently, a carbonate platform gradually evolved with continuous Middle Permian strata distributed widely within the basin. These carbonates are divided into the Liangshan Formation (P_2l), Qixia Formation (P_2q), and Maokou Formation (P_2m), in ascending order [20]. The Emeishan mantle plume activity occurred between the Middle and Late Permian and culminated in the emplacement of the Emeishan large igneous province (ELIP) at ca. 260.1~259.5 Ma [21]. The associated lava basalts can be found throughout most of the southwestern part of the basin and are unconformably overlying the Maokou Formation

(Figure 1) [22]. This magmatic thermal event resulted in abnormally high heat flow of up to 90–110 mW/m^2 in many areas within the basin—especially in its southwestern margin, where the crustal uplift associated with the eruption locally formed highlands and subsequently became denudated [23]. In the subsequent Late Triassic and Cenozoic, the Longmenshan Orogenic Belt along the northwestern margin of the Sichuan Basin experienced multiple periods of thrusting (Figure 1a) [24]. The strong later deformation during this orogenic movement is believed to have played a key role in the formation of the reservoir composed of Permian carbonate rocks in this area [2].

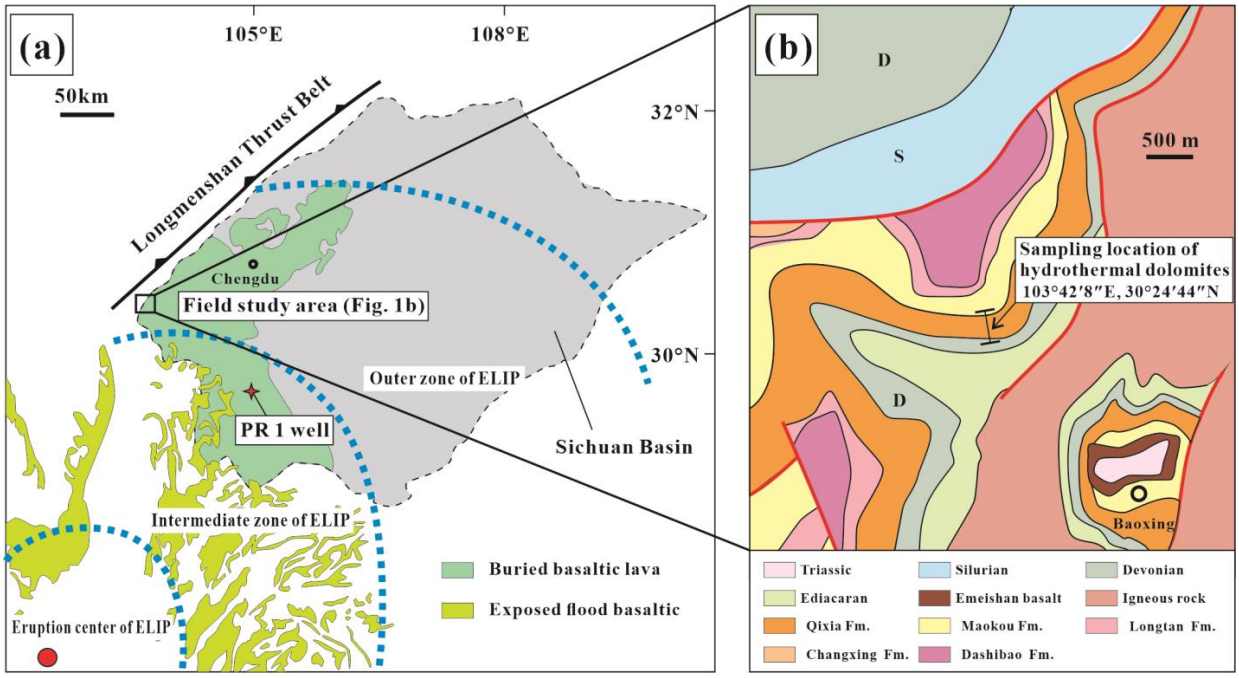


Figure 1. Geological Setting. (**a**) Regional geological settings of the Sichuan Basin (modified based on [22,23]); (**b**) The sampling location of hydrothermal dolomites in the field study area from the Baoxing section.

The Qixia Formation is dominated by marine carbonates with abundant marine fossils. The unit is widely developed across the Sichuan Basin, with a relatively stable thickness of 100 to 200 m. Its depositional age is older than the Emeishan large igneous activity and the Longmenshan orogeny. During the deposition of the lower part of the formation, the sea level rose due to the influence of basin extension. The depositional environment transitioned from a coastal tidal flat to an open platform, with restricted platform and intra-platform beaches and platform-margin shoals developed in the southwestern part of the basin [25]. The upper part of the Qixia Formation reflects a drop in sea level, resulting in a shift of the depositional environments to limited platform and intra-platform shoals within the southwestern and most of the central part of the basin [25]. In our study area in the southwestern Sichuan Basin, one section is proximal to the Longmenshan Orogenic Belt, and the other is within the vicinity of the ELIP (Figure 1a). The depositional environment of the Qixia Formation in this region is dominated by platform-margin shoals and intra-platform shoals. In our study sections, the lower part of the formation is mainly composed of gray-to-dark-gray, thin–thick-layered micritic limestone, bioclastic limestone, and fine–coarse-crystalline dolomite. The upper part of the formation mainly comprises gray thick-layered limestone and gray dolomite. In general, abundant zebra-like hydrothermal dolomites that are distributed along deep and large faults can be found in the lower part of the formation, while saddle dolomites are widely distributed throughout the formation.

3. Samples and Methods

The rock samples used in the present study were taken from the PR1 oil and gas drilling well and the Baoxing section (Figure 1b). While the PR1 well is situated in the intermediate zone of the ELIP, the Baoxing section is more proximal to the Longmenshan Orogenic Belt. Seven samples were collected from each section (P-1, P-5, P-13, P-17, P-19, P-22, and P-28 from the PR1 well, and BX-HTD1, BX -HTD2, BX-HTD3, BX-1, BX-2, BX-6, and BX-11 from the Baoxing section). The replacement dolomites (RDs) and saddle dolomites (SDs) in these samples were the main investigated targets; the occurrence of these hydrothermal dolomites was found to be in close association with the deep and large faults in the study areas. All samples were first examined macroscopically and described, and then they were cut and polished to obtain thin sections. Half of the individual thin sections were stained with alizarin red to identify dolomites. Microscopic observations of these thin sections were carried out with an optical microscope and a CL8200 MK5 cathodoluminescence microscope.

Based on petrological observations, SDs in the P-1 sample (identified as P-1-34 and P-1-42) were selected for in situ carbonate U-Pb dating. The detailed analytical methods and procedures were as described by Roberts and Walker [26], Nuriel et al. [27], and Cheng et al. [28]. In brief, the micro-sampled samples were heated by the laser ablation system using an ablation time of 30 s, a spot size of 100–200 μm, a repetition rate of 15 Hz, and energy of 1.5–3 J/cm^2. The accurate U-Pb isotopic static measurements of the carbonate minerals were then performed by switching a high-sensitivity Faraday cup (10^{12} Ω) and a discrete dynode electron multiplier in Nu Plasma II MC-ICP-MS, using a Tera–Wasserburg diagram in Isoplot software. The $^{238}U/^{206}Pb$-$^{207}Pb/^{206}Pb$ harmony diagram was utilized to determine the U-Pb age of the carbonate minerals [29]. The NIST 614 international glass standard was used to calibrate the reference material $^{207}Pb/^{206}Pb$ and the mass spectrometer $^{238}U/^{206}Pb$ ratio drift [30]; AHX-1d (238.2 ± 0.9 Ma), while LD-5 (75 ± 1.2 Ma) and PTKD-2 (153.7 ± 1.7 Ma) were utilized as laboratory internal standards, and repeated cross-calibration with different standards yielded high reproducibility. The %U-Pb discordance was indicated as described by Roberts et al. [31]. All in situ U-Pb carbonate dating analyses were carried out in the Institute of Geochemistry, Chinese Academy of Sciences (Guizhou), using the ASI RESOlution SE laser ablation system and Nu Plasma II MC-ICP-MS.

SD samples from P-1 (including P-1-39 and P-1-42), P-19, BX-HTD1, BX-HTD2, BX-HTD3, BX-1, and BX-11 were selected for clumped isotope analyses. The sampling was conducted by using a micromill to obtain a fine powder. The acid hydrolysis, purification, and collection of the CO_2 gas were carried out using the automatic clumped isotope preparation instrument (IBEX 2). For each measurement, about 5 mg of the powder samples was weighed and put into a common acid bath. There, the powder was fully reacted with phosphoric acid with a density of 1.92 g/cm^3 at 90 °C. The produced CO_2 was then carried by a helium flow current through a liquid nitrogen cold trap and GC trap for purification. The purified CO_2 was imported into the bellows of a Thermo Fisher Scientific 253 Plus Mass Spectrometer for clumped isotope measurements. Carbon, oxygen, and clumped isotope measurements were performed using this mass spectrometer, equipped with 6 Faraday cups measuring m/z 44–49 and an additional 47.5 cups for monitoring background baselines. We used the carbonate standard ETH to establish a reference frame (ETH-1 = 0.258‰, ETH-2 = 0.256‰, ETH-3 = 0.691‰, and ETH-4 = 0.507‰), then combined the Δ_{47} background calibration to construct an empirical transfer function (ETF), and finally performed a balanced scale CDES transformation in an absolute reference frame to obtain $\Delta_{47\ \text{I-CDES}\ 90\ ^\circ\text{C}}$ [19,32]. The clumped isotope measurements were performed at the Nanjing Institute of Geology and Palaeontology, Chinese Academy of Sciences. The formula for calculating the mineral growth temperature ($T_{\Delta47}$) was as described by Bonifacie et al. [33]. In addition, the corresponding diagenetic fluid's oxygen isotope composition was obtained based on the formula $10^3 \ln\alpha_{\text{dolomite-water}} = 3.14 \times 10^6/T^2 - 3.14$ [34]. Note that the fluid oxygen isotope ($\delta^{18}O_{\text{VSMOW-fluid}}$) values are reported on a V-SMOW scale.

The RD and SD samples P-1, P-5, P-13, P-17, P-22, P-28, BX-1, BX-2, BX-6, and BX-11 were selected for conventional carbon and oxygen isotope analysis. For each measurement, samples were collected using a micromill, and about 500 μg of each sample was fully dissolved in 100% phosphoric acid. The carbon and oxygen isotope compositions ($\delta^{13}C$ and $\delta^{18}O$) of the generated CO_2 were determined using a Thermo Fisher Scientific 253 Plus Mass Spectrometer. All measurements were performed in the Key Laboratory of Petroleum Accumulation Mechanisms, Wuxi, China. All values are reported in per mil relative to V-PDB. Based on internal laboratory standards and standard sample calibration, the precision of analysis was generally better than 0.2‰ for carbon and oxygen isotopes.

4. Results

4.1. Petrographic Characteristics

The original hydrothermal dolomites from the Qixia Formation are mainly composed of grained dolomites and saddle dolomites (Figure 2), with visible cracks of different sizes between 0.1 mm and 1 cm in diameter (Figure 2e). Grain dolomites usually undergo intense alteration and recrystallization, with dark gray replacement dolomite (RD) constituting the matrix of the host rock (Figure 2a–e), associated with floating horn-like debris (Figure 2f). The RDs are mainly composed of fine–medium crystals, with a few fine crystals. Most of the crystals are euhedral–semi-euhedral in shape, with linear contacts dominating, well-developed intercrystalline pores, and some pores filled with saddle-shaped dolomite (SD) (Figure 3a–c). The crystal as a whole emits a uniform dark red light when observed with a cathodoluminescence microscope, indicating that the dolomite formed in the early dolomitization stage, while the intercrystalline pores show obvious harbor-like dissolution edges due to late dissolution and have a bright red light (Figure 3d).

Saddle dolomites (SDs) are white dolomitic cements that grow within cavities or along fractures (Figure 2a,b,d–f). Compared with RDs, SDs have more and larger pores (Figure 3b) and are dominated by medium–coarse crystals, with lower numbers of euhedral crystals, bending crystals, and dirty crystal surfaces (Figure 3e). When observed with a cathodoluminescence microscope, bright red and dark red luminescence can be seen in SDs (Figure 3f), revealing a petrological structure characteristic of multistage dolomitization.

4.2. In Situ U-Pb Ages

In situ U-Pb isotope dating was performed with LA-ICP-MS on SDs (P-1-34 and P-1-42) in sample P-1 and standards (NIST 614, AHX-1d, LD-5, and PTKD-2), and the results are shown in Table 1 and Figure 4. The complete isotope datasets are presented in Table S1. The U contents in P-1-34 and P-1-42 were 36.4–316.5 ppb and 69–6330 ppb, respectively, and the corresponding Pb contents were 11.7–692 ppb and 5.62–5900 ppb, respectively (Table 1). Although the content of ordinary Pb in this sample was similar to that of U, the ratios of 238U/206Pb (0.22–30.4) and 207Pb/206Pb (0.07–0.84) in the laser ablation points varied greatly, which was sufficient to construct a good Tera–Wasserburg reverse isochron line. Finally, the U-Pb absolute dating results (lower intercept ages) from P-1-34 and P-1-42 were 257.9 ± 4.9 Ma (MSWD = 2.4) and 251.0 ± 5.5 Ma (MSWD = 3.4), respectively (Figure 4).

Table 1. LA-ICP-MS U-Pb data of samples and standards.

Samples/ Standards	U (ppb)	Pb (ppb)	$^{238}U/^{206}Pb$	$^{238}U/^{206}Pb$ Prop 2SE	$^{207}Pb/^{206}Pb$	$^{207}Pb/^{206}Pb$ Prop 2SE	Error Correlation	MSWD	Number of Spots
P-1-34	36~317	12~692	0.26~21.3	0.02~2.12	0.15~0.84	0.01~0.07	–0.83~0.58	2.4	147
P-1-42	69~6330	5.6~5900	0.19~24.9	0.04~1.79	0.07~0.81	0.01~0.05	–0.82~1.00	3.4	120
NIST 614	811~838	2294~2356	1.40~1.43	0.125~0.13	0.87~0.88	0.004~0.005	0.12~0.73	—	88
AHX-1d	42~5680	4~1617	2.83~30.68	0.27~3.53	0.05~0.79	0.001~0.037	–0.84~0.67	1.3	79
LD-5	216~1168	5~17	64.1~95.8	6.75~10.92	0.06~0.24	0.006~0.068	–0.11~0.64	0.94	79
PTKD-2	65~121	3~6	32.3~49.8	3.43~5.45	0.06~0.26	0.011~0.034	–0.03~0.99	1.4	79

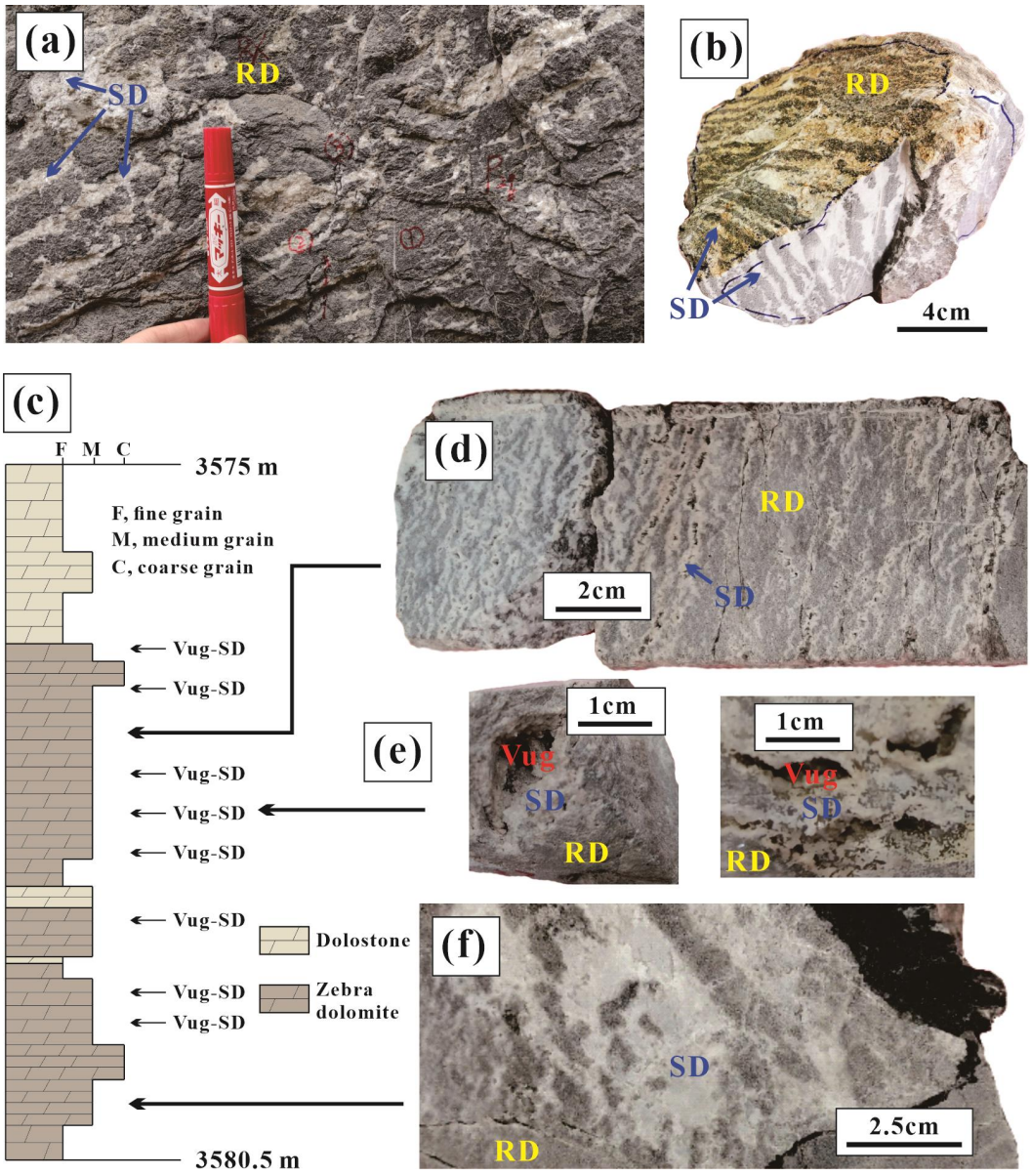


Figure 2. Macro-photographs showing hydrothermal dolomites from the Qixia Formation: (**a**,**b**) Zebra dolomites from the Baoxing outcrop. (**c**) Stratigraphic column in the PR1 well, showing wide distribution of zebra dolomites and vug–saddle dolomites in the Qixia Formation. (**d**) Zebra dolomites from the PR1 well. (**e**) Vug–saddle dolomites from the PR1 well. (**f**) Saddle dolomites containing floating pieces of replacement dolomites.

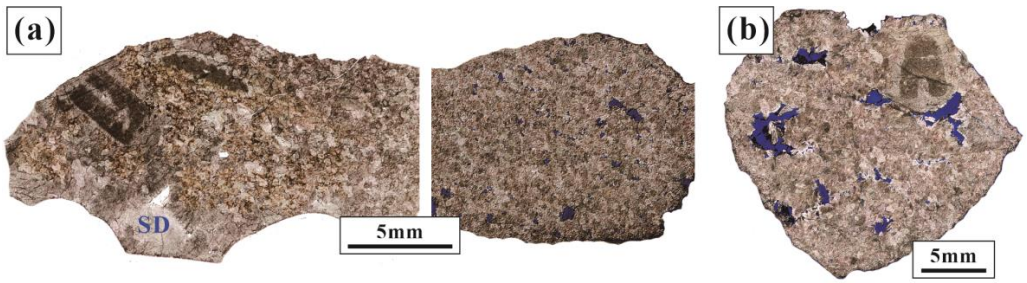


Figure 3. *Cont.*

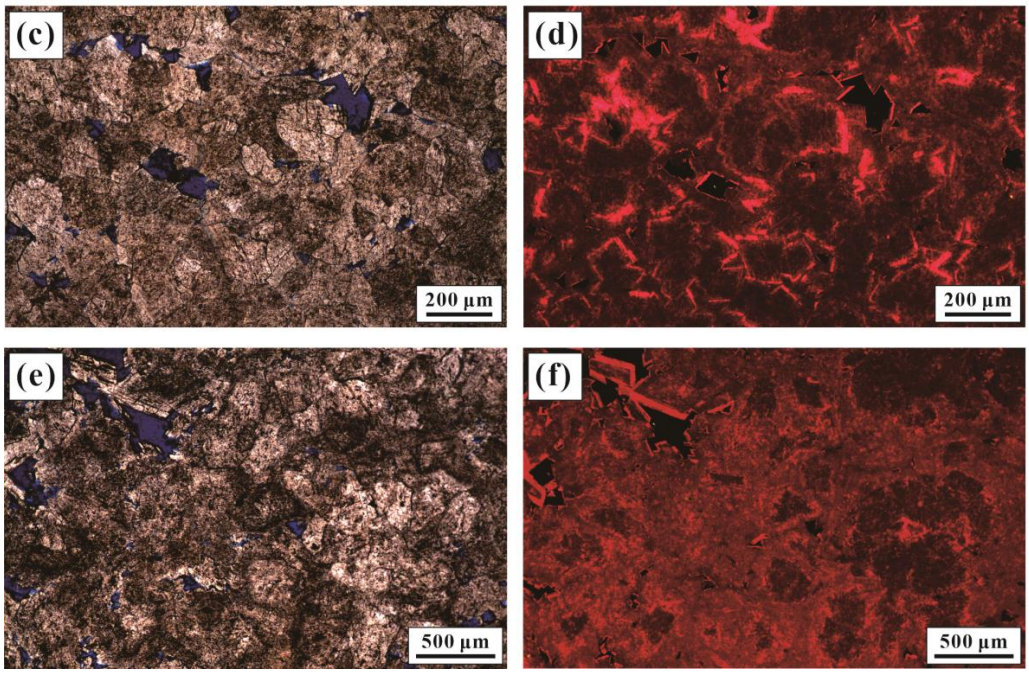


Figure 3. Microphotographs showing hydrothermal dolomites from the Qixia Formation: (**a**) Replacement dolomites from the PR1 well, locally filled with saddle dolomite. (**b**) Saddle dolomites from the Baoxing outcrop, (**c**,**d**) Replacement dolomites from the PR1 well, generally exhibiting a dark red luminescence. (**e**,**f**) Saddle dolomites from the PR1 well, exhibiting a distinguishable bright and dull red luminescence.

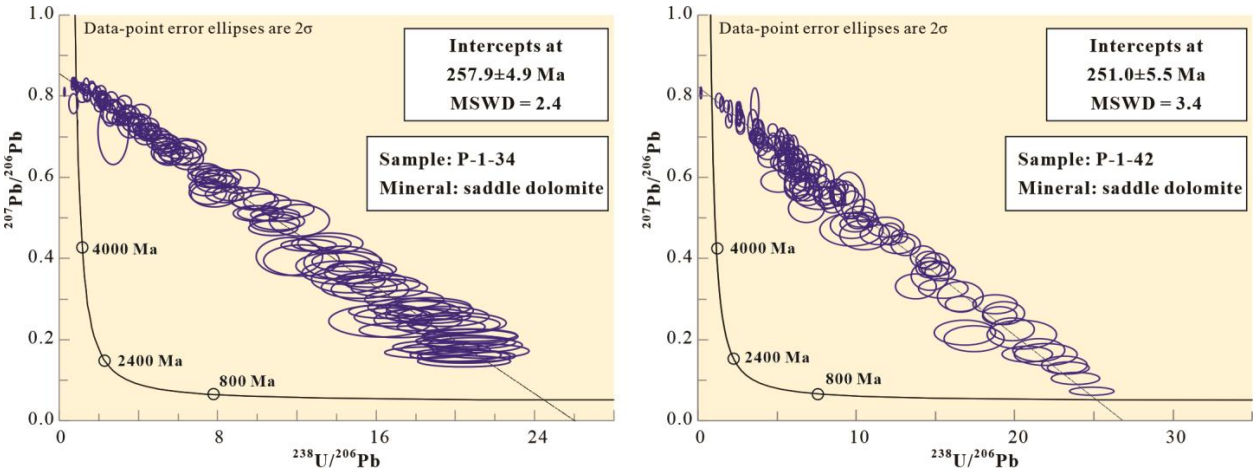


Figure 4. Tera–Wasserburg concordia plots showing $^{238}U/^{206}Pb$ versus $^{207}Pb/^{206}Pb$ of two saddle dolomite samples.

4.3. Carbonate Δ_{47}, $\delta^{13}C$, and $\delta^{18}O$

The results of the clumped isotope analyses for SDs in samples P-1 (including P-1-39 and P-1-42), PR-19, BX-HTD1, BX-HTD2, BX-HTD3, BX-1, and BX-11 are shown in Table 2. These samples were generally measured 2–4 times, and the obtained $\Delta_{47\ \text{I-CDES}\ 90\ ^\circ\text{C}}$ values ranged from 0.297 to 0.470‰. Using the clumped isotope-temperature equation suggested by Bonifacie et al. [33], the calculated $T_{\Delta47}$ for hydrothermal genesis of SDs varied between 77.2 and 223.9 °C. In general, the SDs from the PR1 well had lower $T_{\Delta47}$; samples P-1-39, P-1-42, and P-19 were estimated to have formed at temperatures of 82.2 ± 4.5 °C, 108.4 ± 7.3 °C, and 84.3 ± 1.9 °C (± 1 standard error (SE)), respectively. The SDs from the Baoxing section yielded higher $T_{\Delta47}$, varying between 127.5 ± 9.5 °C and 205.9 ± 9.8 °C

(± 1 SE). Correspondingly, it can be estimated that the diagenetic fluids at the PR1 well had lower $\delta^{18}O_{VSMOW\text{-}fluid}$ values (between −2.92 ± 0.60‰ and 0.81 ± 0.74‰) compared to those at Baoxing, which had higher $\delta^{18}O_{VSMOW\text{-}fluid}$ values (varying from 1.99 ± 0.52‰ to 7.02 ± 0.56‰).

Table 2. Results of the carbonate clumped isotope analyses.

Sample	Mineral	$\delta^{13}C_{VPDB}$ (‰)	$\delta^{18}O_{VPDB}$ (‰)	$\delta^{18}O_{VSMOW}$ (‰) (Dolomite)	$\Delta_{47\ I\text{-}CDES\ 90°C}$ (‰)	$T_{\Delta47}$ (°C)	$T_{\Delta47}$ ± 1SE (°C)	$\delta^{18}O_{VSMOW}$ ± 1 SE (‰) (Fluid)
P-1-39	SD	3.84	−11.35	19.22	0.444	91.25	82.2 ± 4.5	−2.67 ± 0.78
P-1-39	SD	3.83	−11.59	18.97	0.468	78.22		
P-1-39	SD	3.83	−11.76	18.80	0.470	77.20		
P-1-42	SD	4.45	−11.05	19.53	0.398	120.88	108.4 ± 7.3	1.33 ± 0.97
P-1-42	SD	4.46	−11.26	19.31	0.437	95.33		
P-1-42	SD	4.52	−11.01	19.57	0.415	109.11		
P-19	SD	4.11	−11.26	19.31	0.453	86.20	84.3 ± 1.9	−2.28 ± 0.54
P-19	SD	3.85	−11.78	18.78	0.460	82.41		
BX-HTD1	SD	1.67	−12.62	17.91	0.316	198.38	181.7 ± 16.7	7.53 ± 0.38
BX-HTD1	SD	2.55	−10.99	19.59	0.346	165.02		
BX-HTD2	SD	1.96	−13.49	17.01	0.362	149.89	151.3 ± 1.4	3.14 ± 0.18
BX-HTD2	SD	1.68	−14.08	16.41	0.359	152.61		
BX-HTD3	SD	1.63	−12.13	18.42	0.377	137.05	127.5 ± 9.5	2.68 ± 0.82
BX-HTD3	SD	2.55	−11.75	18.81	0.402	118.01		
BX-1	SD	2.68	−12.76	17.77	0.297	223.91	205.9 ± 9.8	7.02 ± 0.65
BX-1	SD	2.66	−12.71	17.81	0.316	198.38		
BX-1	SD	2.79	−12.62	17.91	0.300	219.61		
BX-1	SD	2.33	−13.03	17.49	0.330	181.89		
BX-11	SD	2.54	−12.41	18.13	0.312	203.43	196.5 ± 4.7	6.81 ± 0.34
BX-11	SD	2.44	−12.46	18.07	0.316	198.38		
BX-11	SD	2.33	−12.57	17.96	0.325	187.58		

The results of the conventional carbon and oxygen isotope analyses for RD and SD samples from the two sections are shown in Tables 2–4. The $\delta^{13}C$ and $\delta^{18}O$ values for RD samples from the PR1 well ranged from 2.24 to 5.06 ‰ and from −12.45 to −10.11‰, respectively. The $\delta^{13}C$ values of SD samples from the same section were between 3.59 and 4.52 ‰, with $\delta^{18}O$ values varying between −12.35 and −9.85 ‰. In the Baoxing section, the $\delta^{13}C$ and $\delta^{18}O$ values ranged from 2.83 to 4.39 ‰ and from −15.45 to −9.17 ‰ for RD samples, respectively, and from 1.63 to 2.92 ‰ and from −14.81 to −10.99‰ for SD samples, respectively. In general, the RD and SD samples from the Baoxing section yielded relatively lower $\delta^{13}C$ and $\delta^{18}O$ values compared to those from the PR1 well.

Table 3. Results of the stable isotope ($\delta^{13}C$ and $\delta^{18}O$) analyses of RDs from the PR1 well.

Sample	Mineral	$\delta^{13}C_{VPDB}$ (‰)	$\delta^{18}O_{VPDB}$ (‰)	Sample	Mineral	$\delta^{13}C_{VPDB}$ (‰)	$\delta^{18}O_{VPDB}$ (‰)
P-1-M1	RD	2.24	−12.45	P-13-C2	SD	4.05	−11.08
P-1-M2	RD	3.54	−12.05	P-17-M1	RD	3.89	−10.73
P-1-M3	RD	4.57	−11.35	P-17-C1	SD	3.89	−11.17
P-1-M4	RD	4.14	−11.71	P-17-C2	SD	3.92	−10.56
P-1-C1	SD	3.59	−12.13	P-22-M1	RD	4.35	−10.46
P-1-C2	SD	3.82	−12.11	P-22-C1	SD	4.15	−11.42
P-5-M1	RD	4.95	−11.38	P-22-C2	SD	3.72	−11.87
P-5-M2	RD	5.06	−10.63	P-28-1-M1	RD	4.30	−11.27
P-5-M3	RD	4.05	−12.05	P-28-1-C1	SD	4.30	−11.78
P-13-M1	RD	3.87	−10.98	P-28-1-C2	SD	4.03	−12.35
P-13-C1	SD	3.86	−9.85	P-28-2-M1	RD	4.39	−10.11

Table 4. Results of the stable isotope ($\delta^{13}C$ and $\delta^{18}O$) analyses of RDs from the Baoxing outcrop.

Sample	Mineral	$\delta^{13}C_{VPDB}$ (‰)	$\delta^{18}O_{VPDB}$ (‰)	Sample	Mineral	$\delta^{13}C_{VPDB}$ (‰)	$\delta^{18}O_{VPDB}$ (‰)
BX-1-M	RD	2.83	−14.75	BX-6-M	RD	3.43	−9.17
BX-1-D1	SD	1.71	−12.61	BX-6-D	SD	2.92	−11.74
BX-1-D2	SD	2.54	−11.60	BX-11-M	RD	4.39	−9.33
BX-2-M	RD	2.98	−15.45	BX-11-D	SD	2.32	−12.78
BX-2-D	SD	2.41	−14.81				

5. Discussion

5.1. Preservation of Primary Geochemical Signals

5.1.1. Assessment of the Low-U Dolomite Dating

Since the contents of U and Pb in diagenetic carbonate minerals are usually very low (1 ppb to 1 ppm), the analytical error of the $^{238}U/^{206}Pb$ and $^{207}Pb/^{206}Pb$ ratios is relatively large, leading to a larger uncertainty in the calculated U-Pb ages. In this study, only two successful U-Pb ages were obtained from SDs (P-1-34 and P-1-42)—in sample P-1 from the PR1 well. The $^{238}U/^{206}Pb$ and $^{207}Pb/^{206}Pb$ ratios of the two SDs both yielded good linear sequences on the Tera–Wasserburg concordia plot (Figure 4).

Closed U-Pb isotopic systematics are the most important prerequisite for determining the validity of LA-ICP-MS U-Pb absolute isotopic ages. Carbonate rocks may suffer from potential post-sedimentary superposition during burial diagenesis or thermal events, which may interfere with or reset the U and Pb isotopic signals [35,36]. Here, the presence or absence of open system behavior in each dataset is evaluated mainly through the isotopic data themselves. First, if multiple diagenetic fluid sources are present, the mixed common Pb in dating dolomite cements will limit the derivation of a single age regression line. At the same time, an obviously open system behavior may lead to more scattered U-Pb data and higher mean square of weighted deviates (MSWD) values. Secondly, in the case of diagenetic superposition or fluid interaction with the original carbonate rocks, the Y-intercept (initial $^{207}Pb/^{206}Pb$) of the mixing line of the two diagenetic fluid sources is usually lower than 0.8~0.9 because of the slope change in the regression two-component mixing line [37]. In this study, both U-Pb isotope data points defined a good single isochron with no significant dispersion and a low MSWD (2.4 and/or 3.4). In addition, the initial $^{207}Pb/^{206}Pb$ ratios in P-1-34 and P-1-42 were both higher than 0.8, and the overall isochron line convergence was good. We can thus conclude that the U-Pb isotopic systematics of P-1-34 and P-1-42 did not experience obvious post-deposition alteration and significant influence by mixed fluids. The obtained ages of 257.9 ± 4.9 Ma and 251.0 ± 5.5 Ma, respectively, can thus be interpreted as representing the absolute age of SD deposition.

5.1.2. Evaluating the Potential for Alteration of Δ_{47}

The reconstruction of the carbonate formation temperature with the clumped isotope thermometry can be significantly affected by high-temperature modification [38]. As the carbonate minerals are heated, the solid diffusion of oxygen and/or carbon atoms throughout the mineral lattice will change Δ_{47}, which is in equilibrium with the ambient burial temperature [39,40]. This re-equilibrium or reordering is controlled by thermal dynamics, and its rate and magnitude depend on temperature and temperature action time, which can be demonstrated and reconstructed using thermal history reordering models [39,40].

According to the thermal burial history of the PR1 well, the Qixia Formation at this locality was buried nearly 1km deep in the Late Permian, and the burial temperature was close to 60 °C. The maximum burial depth was reached ca. 100 Ma, with a corresponding burial temperature as high as 150 °C. Subsequently, the rocks were uplifted and cooled to 130 °C (Figure 5a,b). For the Qixia Formation in the Baoxing section near the Longmenshan Orogenic Belt, the thermal burial history was proposed by Pan et al. [10,11]. Based on this,

we can assume that its burial temperature was higher than 120 °C in the Late Permian, and that the maximum burial temperature was nearly 180 °C at ca. 100 Ma. Today, the temperature above the surface is 25 °C (Figure 5c,d). Under these temperature–time path conditions, the solid-state reordering models of Passey and Henkes [39] and Stolper and Eiler [40] were applied in this study, respectively (Figure 5). The results show that regardless of the model used, the temperature–time paths of the Qixia Formation do not exert a significant impact on the $T_{\Delta 47}$, with the maximum change in $T_{\Delta 47}$ being less than 10 °C, indicating that solid-state reordering in hydrothermal dolomites rarely occurs. Based on this, the formation fluid $\delta^{18}O_{VSMOW\text{-}fluid}$ values calculated from the $T_{\Delta 47}$ value can be considered reliable.

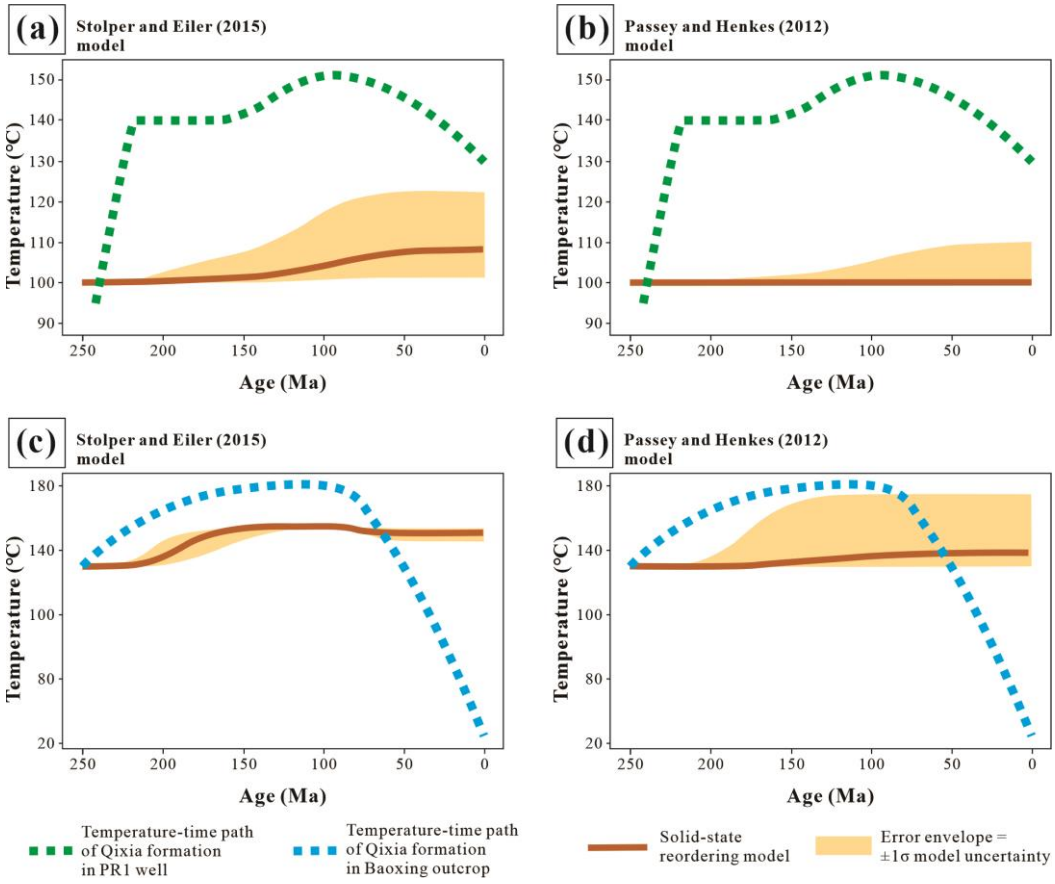


Figure 5. Temporal trends of $T_{\Delta 47}$ determined by solid-state reordering models [39,40], based on temperature–time paths from (**a**,**b**) the PR1 well and (**c**,**d**) the Baoxing section.

5.2. Tectonic Thermal Events Corresponding to the Formation of Hydrothermal Dolomites

The new U-Pb age data obtained in this study show that SDs crystallized in the PR1 well between 257.9 and 251.0 Ma. Notably, previous zircon U-Pb dating indicated that volcanism in the late Middle Permian (i.e., the ELIP) began at ~262 Ma, with the main phase of basalt eruptions occurring between 260.1 Ma and 259.5 Ma [21]. However, the fade of the main eruption phase does not necessarily mean the abrupt end of the plutonic magmatism. Many zircon U-Pb ages indicate that the magmatism and the influence of the ELIP may have continued until the Early Triassic (ca. 251 Ma) [41]. Influenced by the terrain uplift associated with the ELIP, the paleo-heat flow in the Sichuan Basin was up to 60–80 mW/m^2 at ca. 259 Ma, with the highest value reaching 100 mW/m^2 in the southwestern part of the basin. This high paleo-heat flow was maintained until the end of the Permian [42]. The large-scale eruption of Emeishan basalts may have resulted in the development of extensional basement faults in the basin, and the fractures associated with these basement faults might have provided fast migration channels for dolomitization

fluids. Therefore, considering that the PR1 well is in the intermediate zone of the ELIP, and that the SD formation time coincided with the late stage of the Emeishan volcanic activity, the formation of SDs in this well may have been closely linked to the ELIP. In addition, according to the thermal burial model for the well, it is estimated that the burial depth of the Qixia Formation during this period was less than 1 km and the burial temperature was close to 60 °C (Figure 6), which is lower than our reconstructed $T_{\Delta 47}$ (between 82.2 and 108.4 °C), indicating that the SDs may have been influenced by higher-temperature hydrothermal fluids. This observation implies a complex history of thermal evolution for the Qixia Formation in the PR1 well that is closely related to the ELIP.

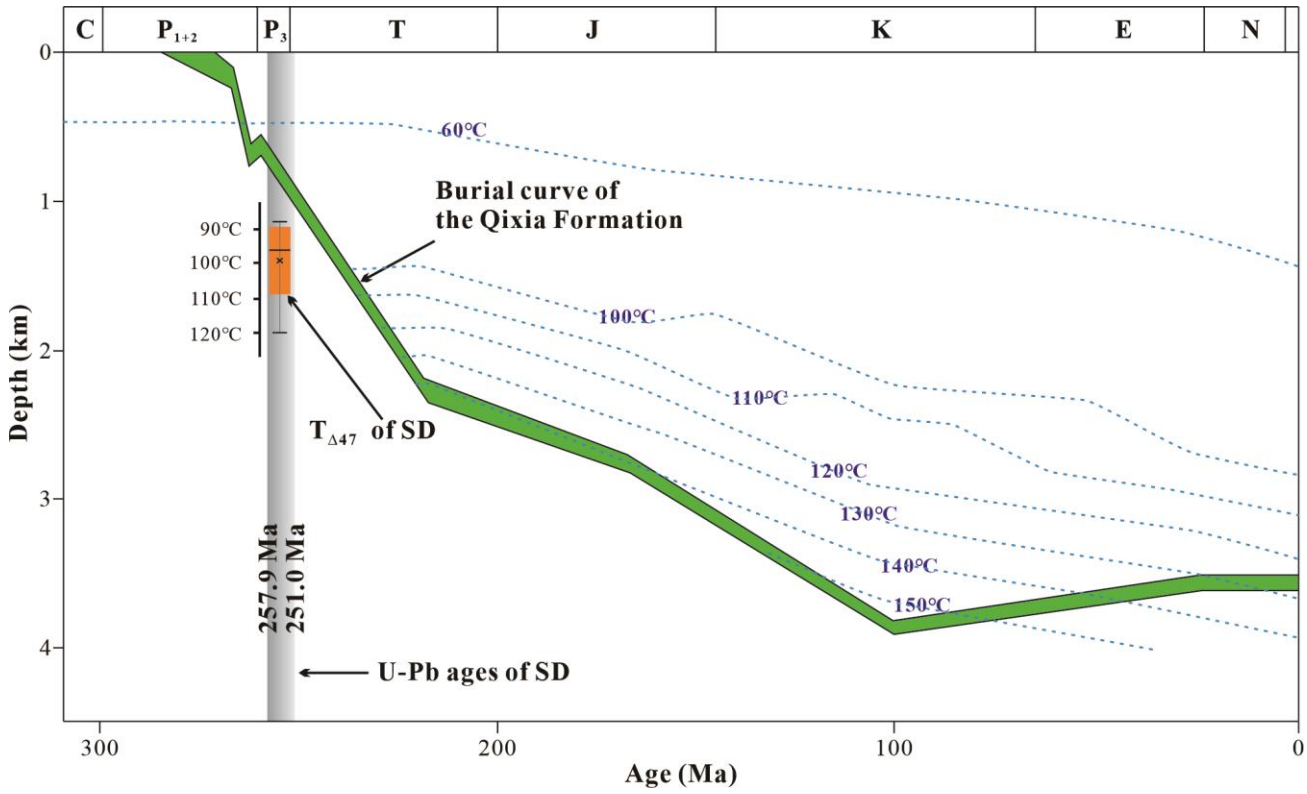


Figure 6. Burial and thermal evolution curves of the Qixia Formation in the PR1 well.

In contrast to the PR1 well, the Baoxing section in the western margin of the Sichuan Basin is situated in the outer zone of the ELIP, but proximal to the southern Longmenshan Orogenic Belt (Figure 1). Pan et al. [11] proposed that the formation age of dolomites (including RDs and SDs) in the Qixia Formation from the western margin of the Sichuan Basin was between 216.4 ± 7.7 Ma and 206 ± 15 Ma based on in situ U-Pb carbonate dating data. These ages are significantly younger than the formation of the ELIP. Similarly, $^{40}Ar/^{39}Ar$ dating of muscovite in the Longmenshan Orogenic Belt shows that thrust activity initiated before the Late Triassic and ended at about 208 Ma [43], coinciding in time and space with the formation of hydrothermal dolomites in the western Sichuan Basin. These observations suggest that the ELIP-related model proposed for the PR1 well may not be applicable for this area. The Longmenshan orogenic activity is thus considered to be a more likely mechanism for the tectonic–hydrothermal dolomite in the Qixia Formation in the Baoxing region [11]. With this orogenic background, the fractures in strata can provide channels for underground high-temperature fluids, pumping deep underground fluids, and promoting the flow of hydrothermal fluids [44]. In addition, our newly obtained $T_{\Delta 47}$ temperatures (127.5~205.9 °C) for SDs from the Baoxing section, along with the dolomite fluid temperatures between 149 and 255 °C estimated by Zheng et al. [4], are significantly higher than the Triassic burial temperatures (85–160 °C) for the Qixia Formation

in this region, providing further evidence to confirm that these dolomites are hydrothermal in origin.

5.3. Diagenetic Model of Hydrothermal Dolomites

5.3.1. Properties of the Diagenetic Fluids

The dissolution and recrystallization caused by ambient fluids cannot alone explain the large differences in carbon isotope composition within the carbonates. These differences mainly depend on changes in the carbon source. As shown in Figure 7, RDs and SDs of the Qixia Formation in the southwestern Sichuan Basin exhibit similar $\delta^{13}C$ and $\delta^{18}O$ values. The $\delta^{13}C$ values (1.63‰~5.06‰) are comparable to those of Middle Permian seawater (ca. 4‰) [45] and the average of Middle Permian marine carbonates (2.86‰, n = 78) in the Upper Yangtze area, but significantly different from mantle-derived carbon, which usually has extremely negative values (<−6‰) [46]. Thus, the $\delta^{13}C$ data suggest that the hydrothermal dolomites were more likely to be influenced by seawater-derived fluids. This is consistent with previous conclusions based on strontium isotopes and rare-earth element (REE) data. In both studied sections, REEs show similarities with modern seawater composition (low REE deficiency), whereas the $^{87}Sr/^{86}Sr$ values are comparable to or slightly higher than those of Middle Permian seawater [47]. Considering that REEs and strontium isotopes in carbonates have good inheritance, this indicates that the late hydrothermal fluids in both sections are mainly derived from a marine rather than a magmatic origin. More importantly, the $\delta^{13}C$ and $\delta^{18}O$ values presented in this study show a similar range for all analyzed hydrothermal dolomites of the Qixia Formation from the southwestern Sichuan Basin (Figure 7), which may suggest a common characteristic of the diagenetic fluids in this area and a general marine source of the fluids.

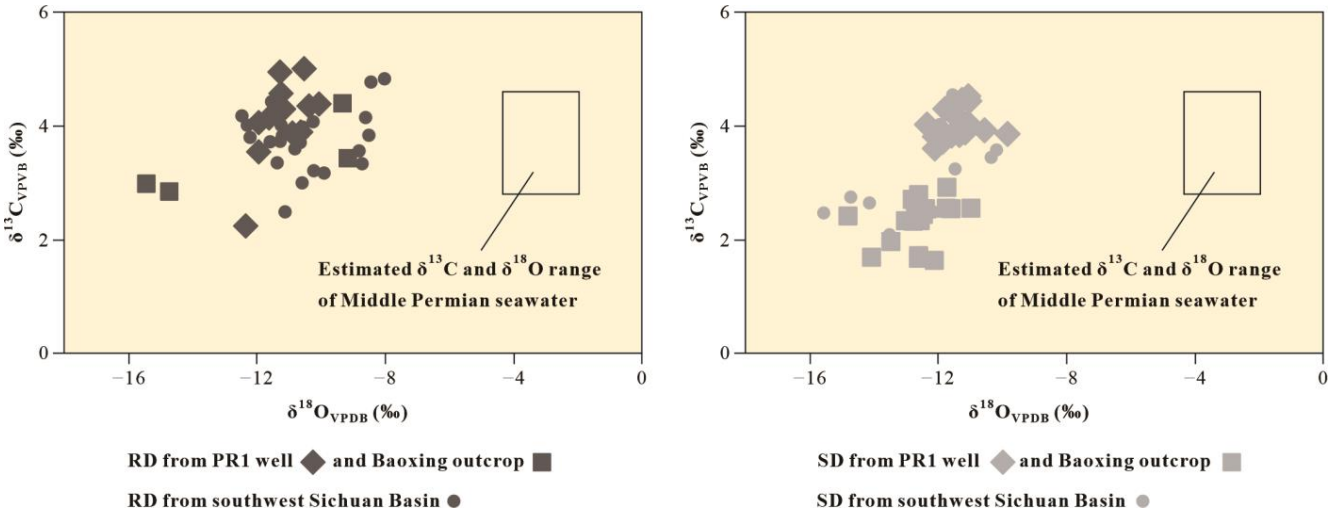


Figure 7. $\delta^{13}C_{VPDB}$ and $\delta^{18}O_{VPDB}$ of RDs and SDs in the Qixia Formation from this study and the southwestern Sichuan Basin (previous data were summarized by Li et al. [9]).

The oxygen isotope composition in carbonates depends on the $\delta^{18}O_{VSMOW\text{-}fluid}$ values and the water–rock exchange interaction during the formation process. During the carbonate formation or the later water–rock exchange interaction, the ambient temperature can significantly affect the oxygen isotope composition, with higher temperatures resulting in lower oxygen isotope values recorded by minerals. This relationship can be expressed by an equation ($10^3 \ln\alpha_{dolomite\text{-}water} = 3.14 \times 10^6/T^2 - 3.14$) [34], and the O isotope composition ($\delta^{18}O_{VSMOW\text{-}fluid}$) compatible with the estimated temperature is presented in Figure 8. Therefore, the low $\delta^{18}O$ values (−15.45‰ to −9.17‰) measured from our hydrothermal dolomites may indicate that they were formed at abnormally high diagenetic temperatures. In comparison to the PR1 well, the $\delta^{18}O$ values of hydrothermal dolomites from the Baoxing section were relatively lower, which may suggest that hydrothermal diagenetic processes

in this section occurred at higher temperatures. A similar phenomenon has been reported from the Cretaceous Bekhme Formation in the Kurdistan region of Iraq, where buried sediments were altered by hydrothermal fluids, with dolomites yielding very low $\delta^{18}O$ values [48].

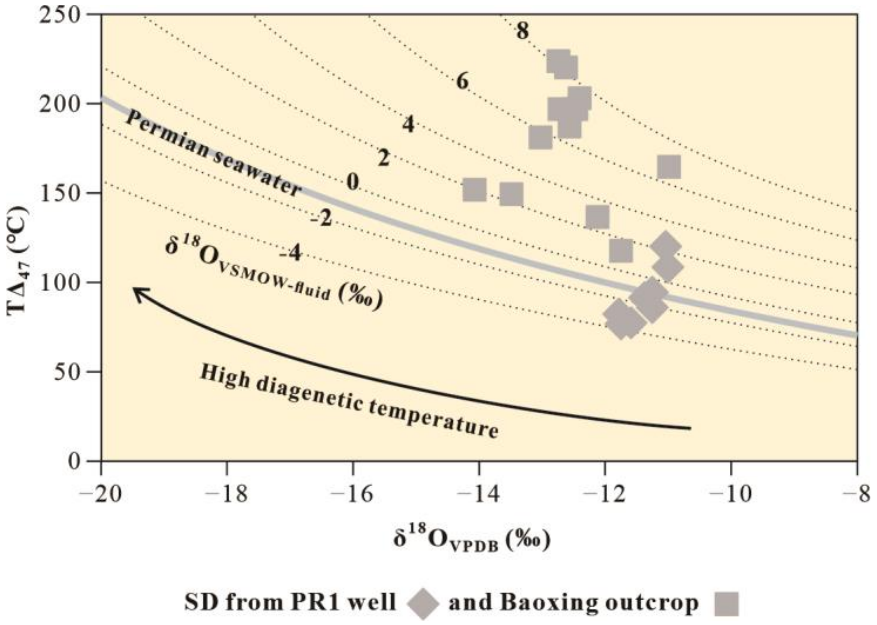


Figure 8. Plot of $\delta^{18}O_{VPDB}$ versus $T_{\Delta 47}$ for SDs. $\delta^{18}O_{VSMOW\text{-}fluid}$ was calculated using the equation of Horita [34].

In addition, the calculated $\delta^{18}O_{VSMOW\text{-}fluid}$ values of diagenetic fluids (−2.92 ± 0.60‰ to 0.81 ± 0.74‰; Figure 8) in the PR1 well were similar to those of coeval seawater (ca. −1.0‰) [49,50], indicating a marine origin. In contrast, the calculated $\delta^{18}O_{VSMOW\text{-}fluid}$ values for the Baoxing section were relatively high (1.99 ± 0.52‰ to 7.02 ± 0.56‰; Figure 8), indicating that the marine-derived fluids at this locality were more salty and, therefore, more enriched in ^{18}O. However, the overall high $\delta^{18}O_{VSMOW\text{-}fluid}$ values might also indicate that the marine fluids were influenced by magmatic hydrothermals ($\delta^{18}O > 6$‰) [46] or other hydrothermal fluids. In fact, $^{87}Sr/^{86}Sr$ ratios higher than in contemporaneous seawater and the high salinity inferred from fluid inclusions in the Baoxing section and surrounding areas indicate features of crust-derived brines [11]. Nevertheless, it should be noted that most alkaline brines may have multiple sources, including marine and meteoric waters, clay mineral dehydration, and magmatic fluids [51]. Moreover, the potential impacts of various or different stages of fluids could lead to wide ranges in the temperature estimates and O isotope values mentioned above.

Based on the above discussion, it is suggested that although the hydrothermal dolomites of the Qixia Formation in the PR1 well were formed during the ELIP activity in the Middle and Late Permian, the associated diagenetic fluids did not originate from the related magmatic activity. The abnormal thermal events caused by Emeishan mantle plume uplift only provided the heat for dolomitization, whereas the fluid source was seawater. In addition, the diagenetic fluids in the southwestern Sichuan Basin were mainly derived from seawater, possibly mixed with other fluids, and then they were captured under the process of stratigraphic burial to form concentrated saline seawater and, finally, form high-temperature hydrothermal fluids under the influence of the ELIP or Longmenshan tectonic thermal events.

5.3.2. Hydrothermal Dolomitization Process

The depositional setting for the Qixia Formation in the southwestern Sichuan Basin was mainly characterized by a restricted platform, inner platform shoal, and platform-margin shoal [25]. The dolomitization of the rocks mainly resulted from penecontemporaneous reflux infiltration, forming microcrystalline dolomite (Figure 9a) [5]. Then, during the early diagenesis and at a shallow burial depth, tectonic thermal events heated the strata and the seawater contained within these strata to form high-temperature hydrothermal fluids. These fluids then intensely interacted with the quasi-syngenetic dolomite, promoting further dolomitization, resulting in the formation of euhedral and semi-euhedral fine crystalline replaced dolomite (RD). Subsequently, cementation mainly occurred in the zebra ridges, hydraulic fractures, and dissolution pores formed by earlier fault processes, and a large amount of saddle-shaped dolomite (SD) was precipitated (Figure 9a). We reconstructed a spatiotemporal diagenetic model for the hydrothermal dolomites in the Qixia Formation in the southwestern Sichuan Basin, which was divided into three stages:

(1) Qixia sedimentary stage (Figure 9b): During the Middle Permian, the Baoxing area at the western margin of the Sichuan Basin was in a platform-margin shoal depositional environment, whereas the PR1 well was situated at an inner platform bank and a restricted platform. Under these quiet and semi-restricted water conditions, the continuous reflux infiltration in the pores of the bank carbonate rocks promoted the formation of quasi-syngenetic dolomite, which provided a good basis for further dolomitization in later stages.

(2) ELIP activity stage (Figure 9c): The Emeishan mantle plume event in the Middle and Late Permian caused rapid differential uplift of the crust on the western margin of the Yangtze Plate, and the top of the Maokou Formation overlying the Qixia Formation was subjected to weathering and denudation [23]. At the same time, mantle plumes caused crustal stretching and extension, and the vicinity of deep and large active faults not only experienced abnormally high temperatures, but also provided a channel for marine fluids [42]. Because the PR1 well and its surrounding areas were in the intermediate zone of ELIP activity, this abnormal thermal event promoted the circulation of diagenetic fluids in the strata, and large-scale hydrothermal dolomitization occurred at shallow burial depths during the Late Permian. Saddle-shaped dolomite cement was deposited and filled in the dissolution holes and fractures of the zebra-like dolomite. However, because the Baoxing area was located at a larger distance from the ELIP activity, it was not significantly affected by this thermal event.

(3) Longmenshan orogenic stage (Figure 9d): In the Late Triassic, the Longmenshan orogeny occurred in the western margin of the Sichuan Basin [24]. The strong thrust caused many strata faults, which could also provide channels for high-temperature marine fluids to circulate, finally causing hydrothermal dolomitization in Baoxing and the surrounding areas proximal to the orogenic belt. Since the PR1 well is situated at a larger distance from the Longmenshan Orogenic Belt, the hydrothermal dolomite in this section does not record this tectonic thermal event.

Overall, the hydrothermal dolomitization in the southwestern Sichuan Basin corresponds well to the neighboring tectonic thermal events in space and time—the ELIP and the Longmenshan orogenic event. Both tectonic thermal events can be demonstrated to have been able to contribute to regional hydrothermal fluid formation, with the saddle-shaped dolomites often distributed along deep fractures. This correspondence illustrates that the hydrothermal dolomitization is mainly associated with coeval penecontemporaneous faulting, which highlights how tectonic movements exert major control over the local hydrothermal field. It is also important for hydrocarbon accumulation, since the dissolution pores that formed under the action of high-temperature hydrothermal activity may provide space for oil and gas and, thus, can serve as a reservoir. In addition, the newly generated deep faults can also provide good hydrocarbon migration channels. These findings provide a new direction for the reservoir research of the Qixia Formation.

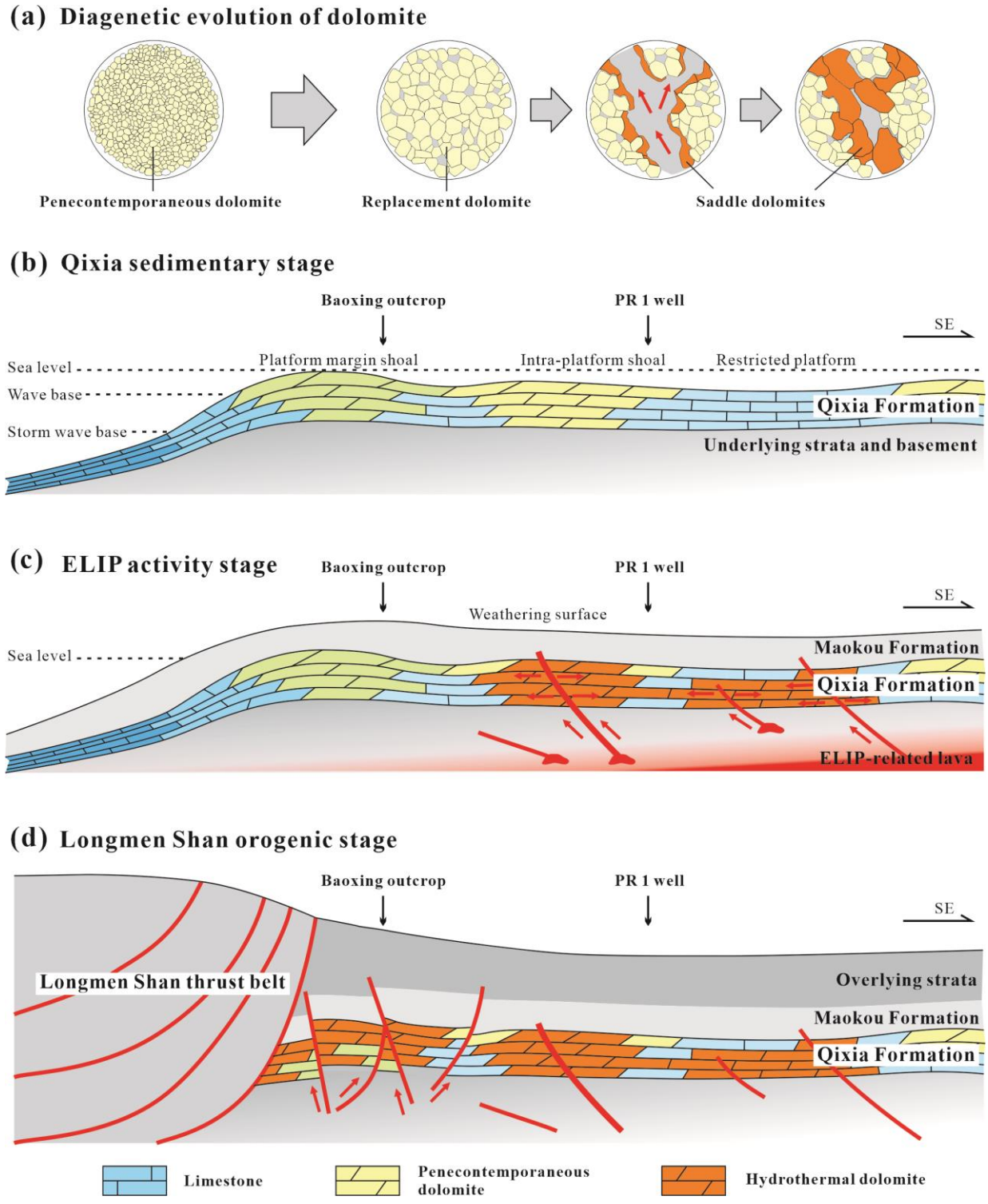


Figure 9. (**a**) Microscopic processes of hydrothermal dolomitization. (**b**–**d**) Diagenetic model for the formation of hydrothermal dolomites of the Qixia Formation, which can be divided into the Qixia sedimentary stage, ELIP activity stage, and Longmenshan orogenic stage, respectively.

6. Conclusions

In this study, the hydrothermal dolomites (RDs and SDs) from the Middle Permian Qixia Formation in the southwestern Sichuan Basin (the PR1 well and Baoxing section) were investigated using in situ U-Pb carbonate dating, clumped isotope analyses, and

classical carbon and oxygen isotope analyses to help understand their properties, sources, and formation history. The major conclusions are as follows:

(1) The in situ U-Pb carbonate dating and Δ_{47} carbonate mineral temperature provide reliable age and formation temperature constraints for the hydrothermal dolomites in the Middle Permian Qixia Formation, confirming the tectonic hydrothermal origin of these dolomites.
(2) The PR1 well is located in the intermediate ELIP zone and at a larger distance from the Longmenshan Orogenic Belt. Its SDs yield in situ U-Pb ages that are concurrent to the ELIP activity. In contrast, in the Baoxing area, the hydrothermal dolomites formed mainly during the Triassic Longmenshan Orogenic Belt, indicating that the causes of the formation of hydrothermal dolomites in the southwestern Sichuan Basin varied in time and space.
(3) RDs and SDs from different areas of the Qixia Formation have similar $\delta^{13}C$ and $\delta^{18}O$ values, suggesting that the diagenetic fluids in the southwestern Sichuan Basin were similar in nature. The $\delta^{13}C$, $\delta^{18}O$, strontium isotope, and REE data all indicate that the diagenetic fluids were mainly derived from marine hydrothermal fluids.
(4) The ELIP and Longmenshan orogenic activity produced faults that provided space for the migration of fluids, while thermal events only provided the heat necessary for the formation of dolomites. This observation indicates that contemporaneous tectonic fault activity was the main factor in the formation of hydrothermal dolomites. These faults also provided channels for the migration of oil and gas.

Supplementary Materials: The following supporting information can be downloaded at: https://www.mdpi.com/article/10.3390/min13020223/s1, Table S1: U-Pb dating data.

Author Contributions: Conceptualization, Y.Z. and D.Y.; methodology, Y.Z., D.Y., H.Y. and Z.T.; investigation, Y.Z., D.Y. and B.C.; writing—original draft preparation, Y.Z.; writing—review and editing, Y.Z., B.C., D.L. and L.Z. All authors have read and agreed to the published version of the manuscript.

Funding: This research was funded by the National Natural Science Foundation of China (U19B6003) and the Open Fund from SINOPEC Key Laboratory of Petroleum Accumulation Mechanisms (33550007-21-ZC0613-0065).

Data Availability Statement: Data are available upon reasonable request. The data that support the findings of this study are available upon request from the corresponding author. The data are not publicly available due to privacy or ethical restrictions.

Acknowledgments: We acknowledge Matthias Alberti from Nanjing University for linguistic support.

Conflicts of Interest: The authors declare no conflict of interest.

References

1. Qi, B.; Zhao, Z.A.; He, H.; Huang, H.; Cao, Z. Reservoir effectiveness evaluation based on comprehensive reservoir quality evaluation indexes of well logging: A case study on the Permian Qixia Fm in the western Sichuan Basin. *Nat. Gas Ind. B* **2018**, *5*, 459–465. [CrossRef]
2. Xiao, D.; Wen, L.; Zhang, Y.; Xie, C.; Tan, X.; Cao, J. Natural gas accumulation in the basin–mountain transition zone, northwestern Sichuan Basin, China. *Mar. Pet. Geol.* **2021**, *133*, 105305. [CrossRef]
3. Chen, M. A discussion of the origin of Yangxin dolomite of Lower Permian in Southwest Sichuan. *Acta Sedimentol. Sin.* **1989**, *7*, 45–50.
4. Zheng, H.; Ma, Y.; Chi, G.; Qing, H.; Liu, B.; Zhang, X.; Shen, Y.; Liu, J.; Wang, Y. Stratigraphic and Structural Control on Hydrothermal Dolomitization in the Middle Permian Carbonates, Southwestern Sichuan Basin (China). *Minerals* **2019**, *9*, 32. [CrossRef]
5. Dong, Y.; Chen, H.; Wang, J.; Hou, M.; Xu, S.; Zhu, P.; Zhang, C.; Cui, Y. Thermal convection dolomitization induced by the Emeishan Large Igneous Province. *Mar. Pet. Geol.* **2020**, *116*, 104308. [CrossRef]
6. Chen, X.; Zhao, W.; Zhang, L.; Zhao, Z.; Liu, Y.; Zhang, B.; Yang, Y. Discovery and exploration significance of structure-controlled hydrothermal dolomites in the Middle Permian of the central Sichuan Basin. *Acta Pet. Sin.* **2012**, *33*, 562–569.

7. Lin, P.; Peng, J.; Zhang, L.; Lan, X.; Wang, J.; Xia, Q.; Xia, J. Characteristics of multiple dolomitizing fluids and the genetic mechanism of dolomite formation in the Permian Qixia Formation, NW Sichuan Basin. *J. Pet. Sci. Eng.* **2022**, *208*, 109749. [CrossRef]
8. Li, P.; Zou, H.; Hao, F.; Yu, X.; Wang, G.; Eiler, J.M. Using clumped isotopes to determine the origin of the Middle Permian Qixia Formation dolostone, NW Sichuan Basin, China. *Mar. Pet. Geol.* **2020**, *122*, 104660. [CrossRef]
9. Li, S.; Yang, B.; Han, Y.; Gao, P.; Wo, Y.; He, Z. Hydrothermal dolomitization and its role in improving Middle Permian reservoirs for hydrocarbon accumulation, Sichuan Basin. *Oil Gas Geol.* **2021**, *42*, 1265–1280.
10. Pan, L.; Shen, A.; Zhao, J.-X.; Hu, A.; Hao, Y.; Liang, F.; Feng, Y.; Wang, X.; Jiang, L. LA-ICP-MS U-Pb geochronology and clumped isotope constraints on the formation and evolution of an ancient dolomite reservoir: The Middle Permian of northwest Sichuan Basin (SW China). *Sediment. Geol.* **2020**, *407*, 105728. [CrossRef]
11. Pan, L.; Hu, A.; Liang, F.; Jiang, L.; Hao, Y.; Feng, Y.; Shen, A.; Zhao, J. Diagenetic conditions and geodynamic setting of the middle Permian hydrothermal dolomites from southwest Sichuan Basin, SW China: Insights from in situ U–Pb carbonate geochronology and isotope geochemistry. *Mar. Pet. Geol.* **2021**, *129*, 105080. [CrossRef]
12. Drost, K.; Chew, D.; Petrus, J.A.; Scholze, F.; Woodhead, J.D.; Schneider, J.W.; Harper, D.A.T. An Image Mapping Approach to U-Pb LA-ICP-MS Carbonate Dating and Applications to Direct Dating of Carbonate Sedimentation. *Geochem. Geophys. Geosyst.* **2018**, *19*, 4631–4648. [CrossRef]
13. Li, Q.; Parrish, R.R.; Horstwood, M.S.A.; McArthur, J.M. U–Pb dating of cements in Mesozoic ammonites. *Chem. Geol.* **2014**, *376*, 76–83. [CrossRef]
14. Godeau, N.; Deschamps, P.; Guihou, A.; Leonide, P.; Tendil, A.; Gerdes, A.; Hamelin, B.; Girard, J.-P. U-Pb dating of calcite cement and diagenetic history in microporous carbonate reservoirs: Case of the Urgonian Limestone, France. *Geology* **2018**, *46*, 247–250. [CrossRef]
15. Woodhead, J.; Hellstrom, J.; Pickering, R.; Drysdale, R.; Paul, B.; Bajo, P. U and Pb variability in older 375 speleothems and strategies for their chronology. *Quat. Geochronol.* **2012**, *14*, 105–113. [CrossRef]
16. Hoareau, G.; Claverie, F.; Pecheyran, C.; Paroissin, C.; Grignard, P.-A.; Motte, G.; Chailan, O.; Girard, J.-P. Direct U–Pb dating of carbonates from micron-scale femtosecond laser ablation inductively coupled plasma mass spectrometry images using robust regression. *Geochronology* **2021**, *3*, 67–87. [CrossRef]
17. Eiler, J.M. "Clumped-isotope" geochemistry—The study of naturally-occurring, multiply-substituted isotopologues. *Earth Planet. Sci. Lett.* **2007**, *262*, 309–327. [CrossRef]
18. Ferry, J.M.; Passey, B.H.; Vasconcelos, C.; Eiler, J.M. Formation of dolomite at 40–80 °C in the Latemar carbonate buildup, Dolomites, Italy, from clumped isotope thermometry. *Geology* **2011**, *39*, 571–574. [CrossRef]
19. Bernasconi, S.M.; Müller, I.A.; Bergmann, K.D.; Breitenbach, S.F.M.; Fernandez, A.; Hodell, D.A.; Jaggi, M.; Meckler, A.N.; Millan, I.; Ziegler, M. Reducing Uncertainties in Carbonate Clumped Isotope Analysis Through Consistent Carbonate-Based Standardization. *Geochem. Geophys. Geosyst.* **2018**, *19*, 2895–2914. [CrossRef]
20. Zhou, J.; Yao, G.; Yang, G.; Gu, M.; Yao, Q.; Jiang, Q.; Yang, L.; Yang, Y. Lithofacies paleogeography and favorable gas exploration zones of Qixia and Maokou Fms in the Sichuan Basin. *Nat. Gas Ind. B* **2016**, *3*, 226–233. [CrossRef]
21. Zhu, J.; Zhang, Z.; Santosh, M.; Tan, S.; Jin, Z. Submarine basaltic eruptions across the Guadalupian-Lopingian transition in the Emeishan large igneous province: Implication for end-Guadalupian extinction of marine biota. *Gondwana Res.* **2021**, *92*, 228–238. [CrossRef]
22. Feng, Q.; Qiu, N.; Fu, X.; Li, W.; Liu, X.; Ji, R. Maturity evolution of Permian source rocks in the Sichuan Basin, southwestern China: The role of the Emeishan mantle plume. *J. Asian Earth Sci.* **2022**, *229*, 105180. [CrossRef]
23. Jiang, Q.; Qiu, N.; Zhu, C. Heat flow study of the Emeishan large igneous province region: Implications for the geodynamics of the Emeishan mantle plume. *Tectonophysics* **2018**, *724–725*, 11–27. [CrossRef]
24. Yan, D.-P.; Zhou, Y.; Qiu, L.; Wells, M.L.; Mu, H.; Xu, C.-G. The Longmenshan Tectonic Complex and adjacent tectonic units in the eastern margin of the Tibetan Plateau: A review. *J. Asian Earth Sci.* **2018**, *164*, 33–57. [CrossRef]
25. Huang, H.; He, D.; Li, Y.; Wang, B. The prototype and its evolution of the Sichuan sedimentary basin and adjacent areas during Liangshan and Qixia stages in Permian. *Acta Petrol. Sin.* **2017**, *33*, 1317–1337.
26. Roberts, N.M.W.; Walker, R.J. U-Pb geochronology of calcite-mineralized faults: Absolute timing of rift-related fault events on the northeast Atlantic margin. *Geol. Soc. Am.* **2016**, *44*, 531–534. [CrossRef]
27. Nuriel, P.; Weinberger, R.; Kylander-Clark, A.R.C.; Hacker, B.R.; Craddock, J.P. The onset of the Dead Sea transform based on calcite age-strain analyses. *Geology* **2017**, *45*, 587–590. [CrossRef]
28. Cheng, T.; Zhao, J.; Feng, Y.; Pan, W.; Liu, D. In-situ LA-MC-ICPMS U-Pb dating method for low-uranium carbonate minerals. *Chin. Sci. Bull.* **2020**, *65*, 150–154. [CrossRef]
29. Ludwig, K.R. *Isoplot 3.75: A Geochronological Toolkit for Microsoft Excel. No. 5*; Berkeley Geochronology Center: Berkeley, CA, USA, 2000; 75p.
30. Woodhead, J.D.; Hergt, J.M. A Preliminary Appraisal of Seven Natural Zircon Reference Materials for In Situ Hf Isotope Determination. *Geostand. Geoanal. Res.* **2005**, *29*, 183–195. [CrossRef]
31. Roberts, N.M.W.; Troy Rasbury, E.; Parrish, R.R.; Smith, C.J.; Horstwood, M.S.A.; Condon, D.J. A calcite reference material for LA-ICP-MS U-Pb geochronology. *Geochem. Geophys. Geosyst.* **2018**, *18*, 2807–2814. [CrossRef]

32. Dennis, K.J.; Affek, H.P.; Passey, B.H.; Schrag, D.P.; Eiler, J.M. Defining an absolute reference frame for "clumped" isotope studies of CO_2. *Geochim. Cosmochim. Acta* **2011**, *75*, 7117–7131. [CrossRef]
33. Bonifacie, M.; Calmels, D.; Eiler, J.M.; Horita, J.; Chaduteau, C.; Vasconcelos, C.; Agrinier, P.; Katz, A.; Passey, B.H.; Ferry, J.M.; et al. Experimental calibration of the dolomite clumped isotope thermometer from 25 to 350 °C, and implications for the temperature estimates for all (Ca, Mg, Fe) CO_3 carbonates digested at high temperature. *Geochim. Cosmochim. Acta* **2017**, *200*, 255–279. [CrossRef]
34. Horita, J. Oxygen and carbon isotope fractionation in the system dolomite–water–CO2 to elevated temperatures. *Geochim. et Cosmochim. Acta* **2014**, *129*, 111–124. [CrossRef]
35. Russell, J.; Chadwick, B.; Rao, B.K.; Vasudev, V.N. Whole-rock Pb-Pb isotopic ages of Late Archaean limestones. *Karnataka India. Precambrian Res.* **1996**, *78*, 261–272. [CrossRef]
36. Roberts, N.M.W.; Drost, K.; Horstwood, M.S.A.; Condon, D.J.; Chew, D.; Drake, H.; Milodowski, A.E.; McLean, N.M.; Smye, A.J.; Walker, R.J.; et al. Laser ablation inductively coupled plasma mass spectrometry (LA-ICP-MS) U-Pb carbonate geochronology: Strategies, progress, and limitations. *Geochronology* **2020**, *2*, 33–61. [CrossRef]
37. Su, A.; Chen, H.; Feng, Y.; Zhao, J.; Wang, Z.; Hu, M.; Jiang, H.; Nguyen, A.D. In situ U-Pb dating and geochemical characterization of multi-stage dolomite cementation in the Ediacaran Dengying Formation, Central Sichuan Basin, China: Constraints on diagenetic, hydrothermal and paleo-oil filling events. *Precambrian Res.* **2022**, *368*, 106481. [CrossRef]
38. Lawson, M.; Shenton, B.J.; Stolper, D.A.; Eiler, J.M.; Rasbury, E.T.; Becker, T.P.; Phillips-Lander, C.M.; Buono, A.S.; Becker, S.P.; Pottorf, R.; et al. Deciphering the diagenetic history of the El Abra Formation of eastern Mexico using reordered clumped isotope temperatures and U-Pb dating. *Geol. Soc. Am. Bull.* **2018**, *130*, 617–629. [CrossRef]
39. Passey, B.H.; Henkes, G.A. Carbonate clumped isotope bond reordering and geospeedometry. *Earth Planet. Sci. Lett.* **2012**, *351*, 223–236. [CrossRef]
40. Stolper, D.A.; Eiler, J.M. The kinetics of solid-state isotope-exchange reactions for clumped isotopes: A study of inorganic calcites and apatites from natural and experimental samples. *Am. J. Sci.* **2015**, *315*, 363–411. [CrossRef]
41. Shellnutt, J.G. The Emeishan large igneous province: A synthesis. *Geosci. Front.* **2014**, *5*, 369–394. [CrossRef]
42. Zhu, C.; Xu, M.; Yuan, Y.; Zhao, Y.; Shan, J.; He, Z.; Tian, Y.; Hu, S. Palaeogeothermal response and record of the effusing of Emei basalts in the Sichuan basin. *Chin. Sci. Bull.* **2010**, *55*, 474–482.
43. Yan, D.P.; Zhou, M.F.; Li, S.B.; Wei, G.Q. Structural and geochronological constraints on the Mesozoic–Cenozoic tectonic evolution of the Longmen Shan thrust belt, eastern Tibetan Plateau. *Tectonics* **2011**, *30*, TC6005. [CrossRef]
44. Lacroix, B.; Trav'e, A.; Buatier, M.; Labaume, P.; Vennemann, T.; Dubois, M. Syntectonic fluid-flow along thrust faults: Example of the South-Pyrenean fold-andthrust belt. *Mar. Petrol. Geol.* **2014**, *49*, 84–98. [CrossRef]
45. Korte, C.; Jasper, T.; Kozur, H.W.; Veizer, J. δ18O and δ13C of Permian brachiopods: A record of seawater evolution and continental glaciation. *Palaeogeogr. Palaeoclim. Palaeoecol.* **2005**, *224*, 333–351. [CrossRef]
46. Hoefs, J. *Stable Isotope Geochemistry*, 6th ed.; Springer: Heidelberg, Germany, 2009; pp. 111–115.
47. Zhao, J.; Feng, M.; Shen, A.; Wen, L.; Xu, L.; Wang, X.; Liu, X. Genesis of zebra dolomite of the Middle Permian Qixia Formation in the Southwestern Sichuan Basin: Taking Wulong ourcrop in Baoxing area as an example. *Mar. Orig. Pet. Geol.* **2020**, *25*, 223–233.
48. Mansurbeg, H.; Alsuwaidi, M.; Salih, N.; Shahrokhi, S.; Morad, S. Integration of stable isotopes, radiometric dating and microthermometry of saddle dolomite and host dolostones (Cretaceous carbonates, Kurdistan, Iraq): New insights into hydrothermal dolomitization. *Mar. Pet. Geol.* **2021**, *127*, 104989. [CrossRef]
49. Cummins, R.C.; Finnegan, S.; Fike, D.A.; Eiler, J.M.; Fischer, W.W. Carbonate clumped isotope constraints on Silurian ocean temperature and seawater δ18O. *Geochim. Cosmochim. Acta* **2014**, *140*, 241–258. [CrossRef]
50. Henkes, G.A.; Passey, B.H.; Grossman, E.L.; Shenton, B.J.; Yancey, T.E.; Pérez-Huerta, A. Temperature evolution and the oxygen isotope composition of Phanerozoic oceans from carbonate clumped isotope thermometry. *Earth Planet. Sci. Lett.* **2018**, *490*, 40–50. [CrossRef]
51. Saller, A.H.; Stueber, A.M. Evolution of formation waters in the Permian Basin, United States: Late Permian evaporated seawater to Neogene meteoric water. *AAPG Bull.* **2018**, *102*, 403–428. [CrossRef]

Disclaimer/Publisher's Note: The statements, opinions and data contained in all publications are solely those of the individual author(s) and contributor(s) and not of MDPI and/or the editor(s). MDPI and/or the editor(s) disclaim responsibility for any injury to people or property resulting from any ideas, methods, instructions or products referred to in the content.